Cell

Intestinal mucin is a chaperone of multivalent copper

Graphical abstract

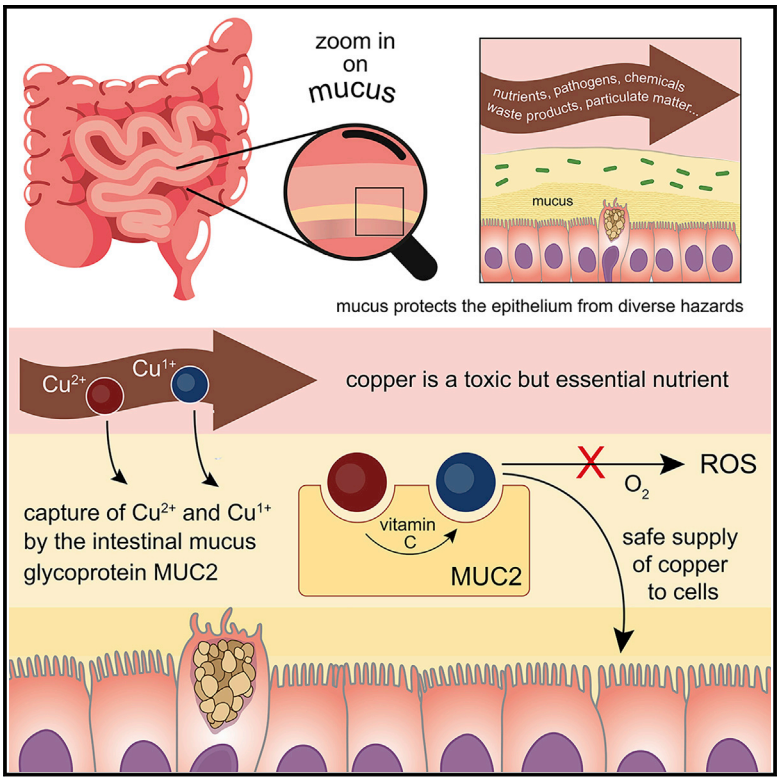

Highlights

- Intestinal and respiratory mucins bind copper at a conserved histidine-rich site
- Copper reduced by vitamin C transits to a methionine-rich site in intestinal mucin
- The mucin copper-binding domain protects intestinal cells from copper toxicity
- Mucin accommodates nutritional copper uptake into cells

Authors

Nava Reznik, Annastassia D. Gallo, Katherine W. Rush, ..., Kelly N. Chacón, Katherine J. Franz, Deborah Fass

Correspondence

deborah.fass@weizmann.ac.il

In brief

Mucins, the major constituents of mucus, protect cells by capturing copper and blocking generation of reactive oxygen species. A two-tiered site in intestinal mucin enables binding of copper in either of its common redox states, which may facilitate safe delivery to cells.

Reznik et al., 2022, Cell *185*, 4206–4215
October 27, 2022
https://doi.org/10.1016/j.cell.2022.09.021

CellPress

CellPress
OPEN ACCESS

Cell

Article

Intestinal mucin is a chaperone of multivalent copper

Nava Reznik,[1] Annastassia D. Gallo,[2] Katherine W. Rush,[3,4] Gabriel Javitt,[1] Yael Fridmann-Sirkis,[5] Tal Ilani,[1] Noa A. Nairner,[1] Simon Fishilevich,[6] David Gokhman,[6] Kelly N. Chacón,[3] Katherine J. Franz,[2] and Deborah Fass[1,7,*]

[1]Department of Chemical and Structural Biology, Weizmann Institute of Science, Rehovot 7610001, Israel
[2]Department of Chemistry, Duke University, Durham, North Carolina 27708, United States
[3]Department of Chemistry, Reed College, Portland, Oregon 97202, United States
[4]Oregon Health & Science University, Portland, Oregon 97239, United States
[5]Life Sciences Core Facilities, Weizmann Institute of Science, Rehovot 7610001, Israel
[6]Department of Molecular Genetics, Weizmann Institute of Science, Rehovot 7610001, Israel
[7]Lead contact
*Correspondence: deborah.fass@weizmann.ac.il
https://doi.org/10.1016/j.cell.2022.09.021

SUMMARY

Mucus protects the epithelial cells of the digestive and respiratory tracts from pathogens and other hazards. Progress in determining the molecular mechanisms of mucus barrier function has been limited by the lack of high-resolution structural information on mucins, the giant, secreted, gel-forming glycoproteins that are the major constituents of mucus. Here, we report how mucin structures we determined enabled the discovery of an unanticipated protective role of mucus: managing the toxic transition metal copper. Using two juxtaposed copper binding sites, one for Cu^{2+} and the other for Cu^{1+}, the intestinal mucin, MUC2, prevents copper toxicity by blocking futile redox cycling and the squandering of dietary antioxidants, while nevertheless permitting uptake of this important trace metal into cells. These findings emphasize the value of molecular structure in advancing mucosal biology, while introducing mucins, produced in massive quantities to guard extensive mucosal surfaces, as extracellular copper chaperones.

INTRODUCTION

Giant mucin glycoproteins are secreted from cells to form protective mucus hydrogels covering the exposed surfaces of internal organs such as the lung and intestine (McGuckin et al., 2011; Benam et al., 2018). These hydrogels guard the underlying epithelium from pathogens and other hazardous matter entering from the outside world, while permitting nutrient absorption and gas exchange. Mucin gels store antimicrobial molecules that participate in innate immunity (Hoffmann, 2021; Padra et al., 2019). Mucin glycoproteins also house and feed the microbiome, lubricate tissue surfaces, and may facilitate the removal of contaminants and waste products from the body (Paone and Cani, 2020). These numerous activities are enabled by the large sizes, dynamic conformations, post-translational modifications, and extensive intermolecular interactions of mucins. However, the same features that contribute to mucin functionality also complicate the study of these glycoproteins. Consequently, many questions remain regarding the mechanisms of mucin assembly, their physical and chemical capabilities, and their physiological contributions to the critical interfaces between animals and their environments.

Using cryo-electron microscopy (cryo-EM), we recently determined the structure of the amino-terminal region of the intestinal mucin, MUC2, in the context of a filament proposed to represent a bioassembly intermediate (Javitt et al., 2020). We noticed in the first von Willebrand factor type D (D1) region of this structure (Figures 1A and 1B) an intriguing congregation of histidine and methionine amino acids, including Met146, Met154, His277, His324, and Met326, arranged with the side chains pointing toward one another. Most of these amino acids are highly conserved in vertebrate MUC2 orthologs (Figure 1C). Inspection of human mucin paralogs revealed that the histidines are found in other gel-forming mucins (i.e., MUC5AC and MUC5B), but the methionines are largely restricted to MUC2 (Figure 1D). In the genetic code, histidine is represented by two codons and methionine by only one, so these amino acids could readily have been replaced in evolution if they were not under strong functional selection.

Histidines and methionines are common copper ligands in proteins (Rubino and Franz, 2012). Copper is bound by proteins as a cofactor in a variety of important redox enzymes, to which it is delivered by dedicated transporters and chaperones in the circulation and in cells (Rubino and Franz, 2012; Linder, 2016; Magistrato et al., 2019). Dysregulation of copper handling due to genetic mutations impairs vascular, hepatic, and immune functions, and deficiency or mis-localization of copper is associated with the pathophysiology of neurodegenerative and other diseases (DiNicolantonio et al., 2018; Acevedo et al., 2019). Despite

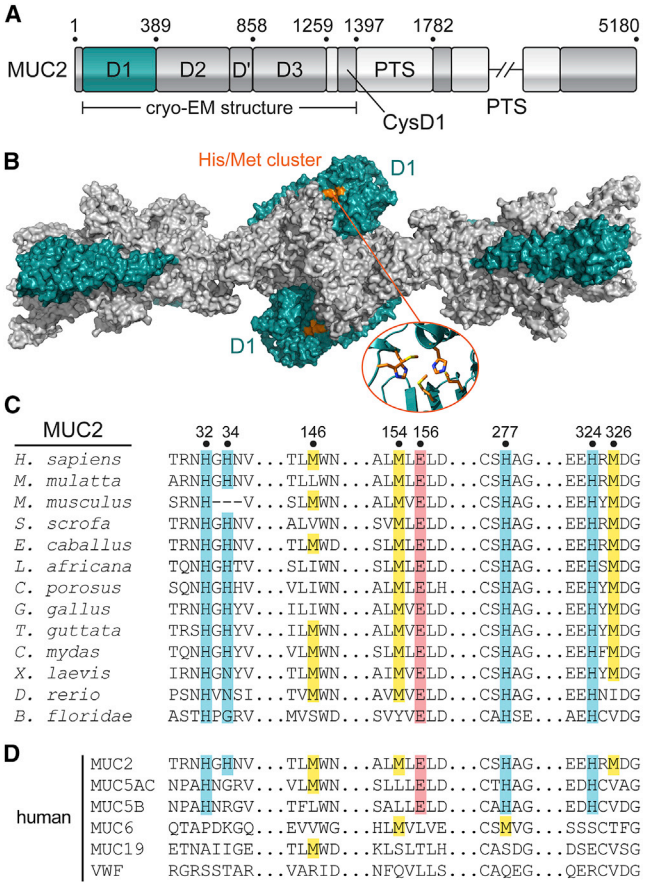

Figure 1. Histidines are conserved in intestinal and respiratory mucins, methionines only in intestinal mucins

(A) Domain map of human MUC2. The D1 assembly is colored teal. "PTS" refers to low-complexity segments rich in proline and O-glycosylated serine and threonine. Numbers indicate amino acid positions at key domain boundaries in the MUC2 precursor (UniProt Q02817).

(B) Filament formed by the amino-terminal region of MUC2 (Javitt et al., 2020), shown as a molecular surface representation. Orange indicates a cluster of histidines and methionines, shown in expanded view in the inset. This and other structure figures were made using Pymol (DeLano, 2002).

(C) An amino acid sequence alignment of MUC2 orthologs from representative animal species was generated, and the segments that include the histidines and methionines are displayed. Histidines at the indicated positions are highlighted in blue, methionines in yellow, and a glutamic acid relevant to this work in pink. The human MUC2 sequence is taken from NCBI NP_002448.4. The lancelet *Branchiostoma floridae* sequence raises the possibility that the histidine cluster predated vertebrates.

(D) Amino acid sequence alignment of human gel-forming mucins and the related blood clotting protein von Willebrand factor (vWF). MUC5B and MUC5AC are gel-forming mucins in airway mucus (Benam et al., 2018).

the importance of copper use and regulation in the body, little is known about the initial encounter with dietary copper or about copper management at mucosal surfaces. This gap is largely due to the heterogeneity of mucosal environments and, as noted above, limited knowledge about the complex macromolecules that function there. Here, we present structural and biochemical evidence that mucins are copper-binding proteins. We show that the intestinal mucin uses distinct coordination sites to engage copper in multiple oxidation states, and we demonstrate the functional benefits of copper regulation by mucin.

RESULTS

Gel-forming mucins bind copper

To test whether MUC2 binds copper, the isolated D1 assembly was prepared, incubated with an equimolar amount of $CuSO_4$, and crystallized (Table S1). The X-ray crystal structure revealed a Cu^{2+} binding site located at the interface of multiple subdomains near the protein surface (Figures 2A and S1A). Though histidines are also prevalent in zinc binding sites (Ireland and Martin, 2019), no evidence of zinc was seen in D1 crystals grown in the presence of $ZnCl_2$ (data not shown). Microscale thermophoresis (MST) metal binding assays in solution supported a preference for Cu^{2+} over a variety of nutrient and non-nutrient metals (Figure S1B), and Zn^{2+} was a poor competitor for Cu^{2+} binding (Figure S1C). MST could not provide an absolute measure of Cu^{2+} affinity in this case because the dissociation constant was substantially below the protein concentration required for the measurements. Isothermal titration calorimetry (ITC) confirmed tight Cu^{2+} binding by D1, and measurements with glycine as a competitor yielded $\log K_D$ values in the range of -12 or -13 depending on solution conditions (Figure S1D and Table S2).

Cu^{2+} was coordinated in the MUC2 D1 crystal structure by three histidines and a glutamate (Figure 2B). In addition to His277 and His324, which drew closer together in the crystal structure compared to their positions in the cryo-EM cluster (Figure 2C), the amino-terminal region of D1 became ordered in the crystal, providing His34 for metal coordination. The highly conserved Glu156 (Figure 1C) completed the Cu^{2+} coordination sphere. Though other proteins bind Cu^{2+} with similar ligands, the MUC2 geometry is distinct (Figure S2). The three histidines occupy approximately three sides of a square-planar coordination geometry, while the glutamate approaches at an angle of about 120° to the plane. The copper ligands were observed at 2.0 to 2.3 Å distance from the metal in the crystal structure model. The three methionines present in the cryo-EM cluster, Met146, Met154, and Met326, did not contribute to Cu^{2+} binding in the D1 crystal structure and were positioned with their sulfur atoms about 6 Å away from the metal (Figure 2B). Extended X-ray absorption fine structure (EXAFS) of Cu^{2+}-loaded MUC2 D1 was consistent with ligation to three multiple scattering histidine residues and one N/O ligand and provided more accurate distances of 2.018 and 1.886 Å for the histidines and glutamate, respectively (Figures 2D, S3A, and Table S3).

Supporting the structural studies, Cu^{2+} addition to MUC2 D1 increased the temperature midpoint of its thermal unfolding transition measured by differential scanning fluorimetry (DSF) (Figures 2E and S4A). This phenomenon was particularly dependent on His277 and His324 but independent of the methionines (Figure 2E). Interestingly, His32, which had a disordered side chain that did not participate in Cu^{2+} ligation in the crystal structure (Figure 2B), is highly conserved across vertebrates (Figure 1C) and invariant in a large-scale study of human genomic sequences (0 alternative alleles in a cohort of 76,156 genomes; gnomAD) (Karczewski et al., 2020), suggesting that mutations at this position are not tolerated and that this histidine plays a critical

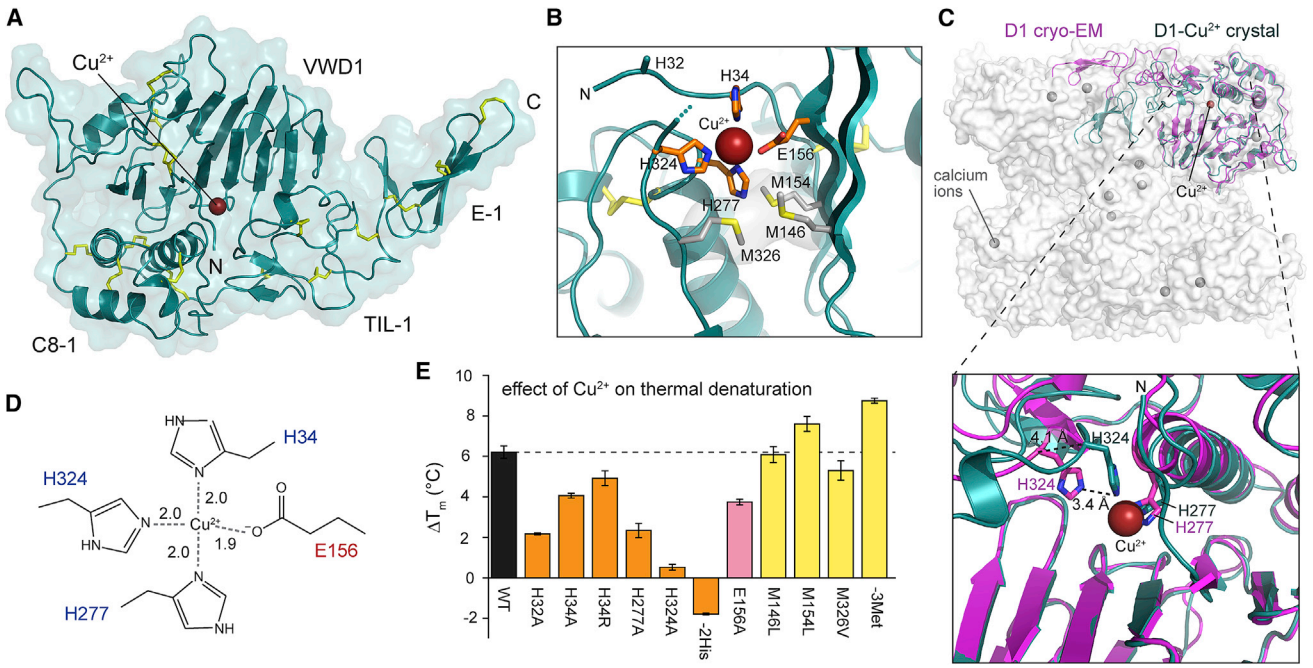

Figure 2. MUC2 binds Cu^{2+}

(A) MUC2 D1 $Cu2^{+}$-bound crystal structure. A backbone cartoon is shown within a semi-transparent surface, and the dark red sphere is the copper ion. Disulfide bonds are yellow. Polypeptide termini are labeled "N" and "C." Domains are labeled according to convention (Nilsson et al., 2014). See also Figure S1.

(B) Ligation of Cu^{2+} in MUC2 D1. Methionines (Met146, Met154, Met326) did not participate in Cu^{2+} coordination, and the Met sulfurs were more than 6 Å from the Cu^{2+}. The His32 side chain was disordered in the crystal. See also Figure S2.

(C) Comparison of the MUC2 D1 crystal structure with D1 in the cryo-EM structure of the filamentous assembly intermediate (Javitt et al., 2020) (Figure 1B). A cartoon representation of one D1 assembly is colored magenta within a semi-transparent surface representation of a unit in the filament (Figure 1B). The crystal structure of MUC2 D1 bound to Cu^{2+} is superposed in dark teal. The D1 assembly is rotated by about 180° compared to (A). Calcium ions bound at specific acidic motifs found in mucins and the related von Willebrand factor are indicated (Dong et al., 2019; Javitt et al., 2019). The zoomed-in view below shows how movement of the TIL1 domain brings His324 closer for Cu^{2+} coordination.

(D) Illustration of the Cu^{2+}-coordination site with ligand-metal distances, rounded to the 10th of an Ångstrom, obtained from EXAFS (Table S3). See also Figure S3.

(E) Cu^{2+} binding increased the midpoint of thermal denaturation of MUC2 D1 by about 6°C (black bar), measured at a protein concentration of 7.5 μM using DSF at pH 5.7. The differences between the denaturation temperatures with and without Cu^{2+} (ΔT_m) are shown for the indicated variants, colored according to amino acid type mutated. His34 was mutated also to arginine because the UniProt entry Q02817 contains arginine at this position. The label "-2His" refers to the double H277A/H324A mutant. The label "-3Met" refers to the triple M146L/M154L/M326V mutant. Data are averages of three separate measurements, and errors are SD.

See also Figures S1, S2, S3, and S4A.

role in MUC2 function. Indeed, the effect on copper-induced thermal stabilization of mutating His32 was similar in magnitude to mutation of the Cu^{2+} ligand His277 (Figure 2E). The impact of mutating His34, seen to bind Cu^{2+} in the crystal (Figure 2B), was more moderate (Figure 2E). Nevertheless, His34 is also invariant in the human population study (Karczewski et al., 2020), despite the appearance of an arginine at this position in the UniProt entry Q02817. As His32 and His34 are found in the flexible, amino-terminal segment of the protein, it is possible that either histidine can participate in copper ligation in a physiological context (i.e., outside a crystal lattice), or that a dynamic process of copper engagement utilizes both histidines.

Importantly, Cu^{2+} increased the midpoint of thermal denaturation also for longer segments of MUC2 (Figure S4B). MUC2 can be cleaved proteolytically *in vivo* to yield the D1D2 segment (Schütte et al., 2014), as we also observed in the murine colon (Figure S4C) and in the supernatant of the LS174T MUC2-producing cell line (Figure S4D). Cu^{2+} binding is therefore displayed by a physiological MUC2 fragment as well as by the full ~1250 amino acid, multiple D-assembly portion at the amino terminus of MUC2 (Figure 1A).

In light of the conservation of the histidines and glutamic acid in other major gel-forming mucins (Figure 1D), we hypothesized that these mucins also coordinate Cu^{2+}. Supporting this hypothesis, D1 of the murine MUC5B ortholog (denoted Muc5b), a representative respiratory mucin, showed increased thermal stability in the presence of Cu^{2+} as measured by DSF (Figure S4E). MST confirmed Muc5b Cu^{2+}-binding activity (Figure S4F).

Reduced copper is captured at a neighboring site in MUC2

Though the MUC2 D1 methionines did not engage in Cu^{2+} coordination (Figure 2B), the proximity of these conserved amino acids to the Cu^{2+} binding site could not be overlooked. Methionines often participate in Cu^{1+} binding (Rubino and Franz, 2012), leading to the hypothesis that MUC2 has distinct sites for Cu^{2+}

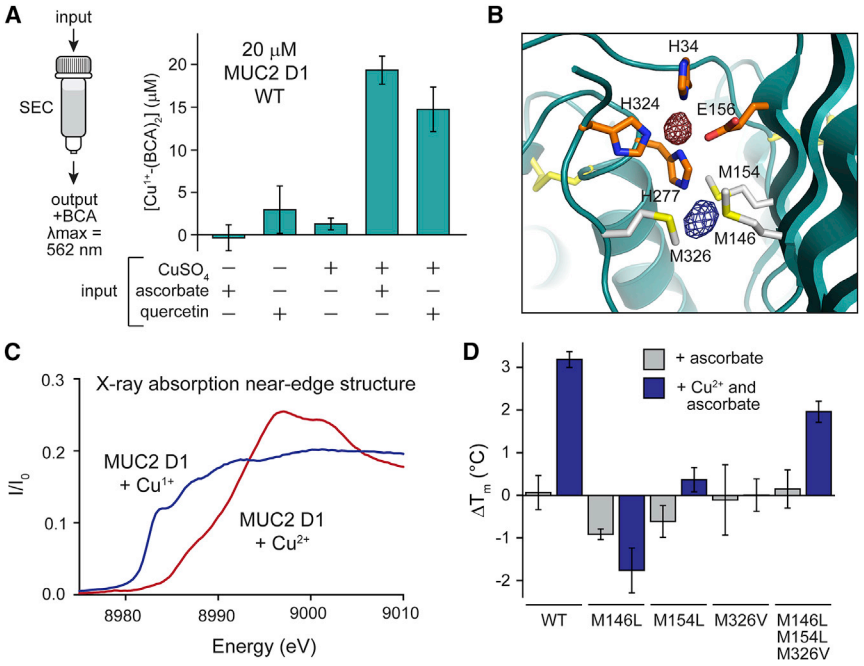

Figure 3. Reduced copper is transferred to a nearby methionine cluster in MUC2

(A) The indicated additions were made to MUC2 D1. Buffer was rapidly exchanged on a size exclusion spin column (SEC) to remove excess reductant or unbound copper, and Cu^{1+} retained by 20 μM protein was detected colorimetrically using the absorbance of the Cu^{1+}-$(BCA)_2$ complex. Data are averages of three separate measurements, and errors are SD.

(B) Fo-Fc difference map density, calculated using the diffraction data from ascorbate-treated MUC2 D1-Cu^{1+} crystals phased using MUC2 D1 coordinates from which the Cu^{2+} ion had been removed. Map is displayed at 4.5σ (dark blue). For comparison, 2Fo-Fc map density of the Cu^{2+} crystal is superposed and displayed at 8σ showing electron density for the Cu^{2+} ion (dark red). The ribbon diagram was made using the coordinates of the Cu^{2+}-bound form without displaying the Cu^{2+}.

(C) Normalized X-ray absorption near-edge structure (XANES) spectrum of MUC2 D1 supplied with $CuSO_4$ is shown in red. The blue spectrum was measured after treatment of the Cu^{2+}-bound MUC2 D1 with ascorbate. The first inflection point of MUC2 D1 Cu^{1+} was calculated to occur at 8982.4 eV, while the first inflection point of MUC2 D1 Cu^{2+} was at 8986.0 eV. See also Figure S3.

(D) Cu^{1+} binding, obtained by providing Cu^{2+} together with ascorbate, increased the midpoint of thermal denaturation of MUC2 D1 by about 3°C, measured at a protein concentration of 12 μM using DSF at pH 5.7. The differences between the denaturation temperature of each variant (ΔT_m) with and without the indicated treatments are shown for wild type (WT) and methionine mutants, demonstrating that the methionines are required for the stabilization against thermal denaturation provided by Cu^{1+}. Data are averages of three separate measurements, and errors are SD.

See also Figures S3, S4E, and S5.

and Cu^{1+}. We found that Cu^{2+} bound by D1 was reduced to Cu^{1+} by ascorbate (vitamin C) and by the dietary flavonoid quercetin (Figure 3A). This observation inspired the addition of ascorbate to the Cu^{2+}-bound MUC2 D1 crystals. Diffraction data collected from these crystals revealed a strong peak of electron density between the methionines, whereas the density corresponding to the histidine-dominated Cu^{2+} site had disappeared (Figure 3B). The resolution of the diffraction data from the ascorbate-treated crystals was not sufficient to precisely measure sulfur-copper distances, but EXAFS of MUC2 D1 in solution confirmed Cu^{1+} binding and provided structural information on the Cu^{1+} coordination environment. Upon treatment of Cu^{2+}-bound MUC2 D1 with ascorbate, the ligation changed dramatically from three-His, one-N/O to three sulfur ligands with an average Cu–S distance of 2.317 Å (Figure S3B and Table S3), which agrees well with data on other methionine Cu^{1+} protein systems (Chacón et al., 2014; Martin-Diaconescu et al., 2016). These changes in coordination environment and redox state were also indicated by the differences in the copper edges of the raw X-ray absorption data (Figure 3C).

Mutagenesis further supported the importance of the methionines in Cu^{1+} binding. Cu^{1+} increased the thermal unfolding transition temperature for MUC2 D1 and longer MUC2 segments to about half the extent as Cu^{2+}, and its effect was entirely undermined by mutating Met146, Met154, or Met326 (Figures 3D and S4E). Furthermore, mutation of methionines lowered the affinity for Cu^{1+}, from a $\log K_D$ of −14 to −12 or below, as measured by competitive titrations (Figure S5). A MUC2 D1 variant with all three methionines mutated to leucine or valine (M146L/M154L/M326V) gave a $\log K_D$ of −13 (Figure S5), in accordance with some thermal stabilization of this variant by Cu^{1+} (Figure 3D). It is possible that the triple mutant binds Cu^{1+} with the aid of some of the histidines when the Cu^{1+} site is eliminated. However, Muc5b, which naturally lacks the methionines but contains the histidines, was not stabilized by Cu^{1+} (Figure S4E). Together, the experiments described thus far provide structural and biochemical evidence for a two-tiered copper binding environment in MUC2, in which histidines dominate the Cu^{2+} coordination and nearby methionines capture Cu^{1+}.

MUC2 blocks ROS formation and protects colon cells from copper toxicity

Copper catalyzes the consumption of oxygen and the formation of reactive oxygen species (ROS) while depleting available antioxidants (Buettner and Jurkiewicz, 1996). To explore the effect of MUC2 on copper-mediated electron transfer, we followed the oxidation of ascorbate in aerobic copper-containing solutions by monitoring the decrease in absorbance at 265 nm (Figure 4A). Although Cu^{2+} bound to MUC2 D1 was reduced by ascorbate (Figure 3A), the bound copper did not undergo futile cycling in the transfer of electrons from ascorbate to oxygen (Figure 4B). Mutation of MUC2 copper ligands compromised the suppression of redox cycling, and Muc5b D1, which lacks a Cu^{1+} binding site, was less effective than MUC2 D1 (Figure 4B). Longer MUC2 segments prevented the redox cycling of copper as effectively as the D1 assembly alone (Figure 4C). These results indicate

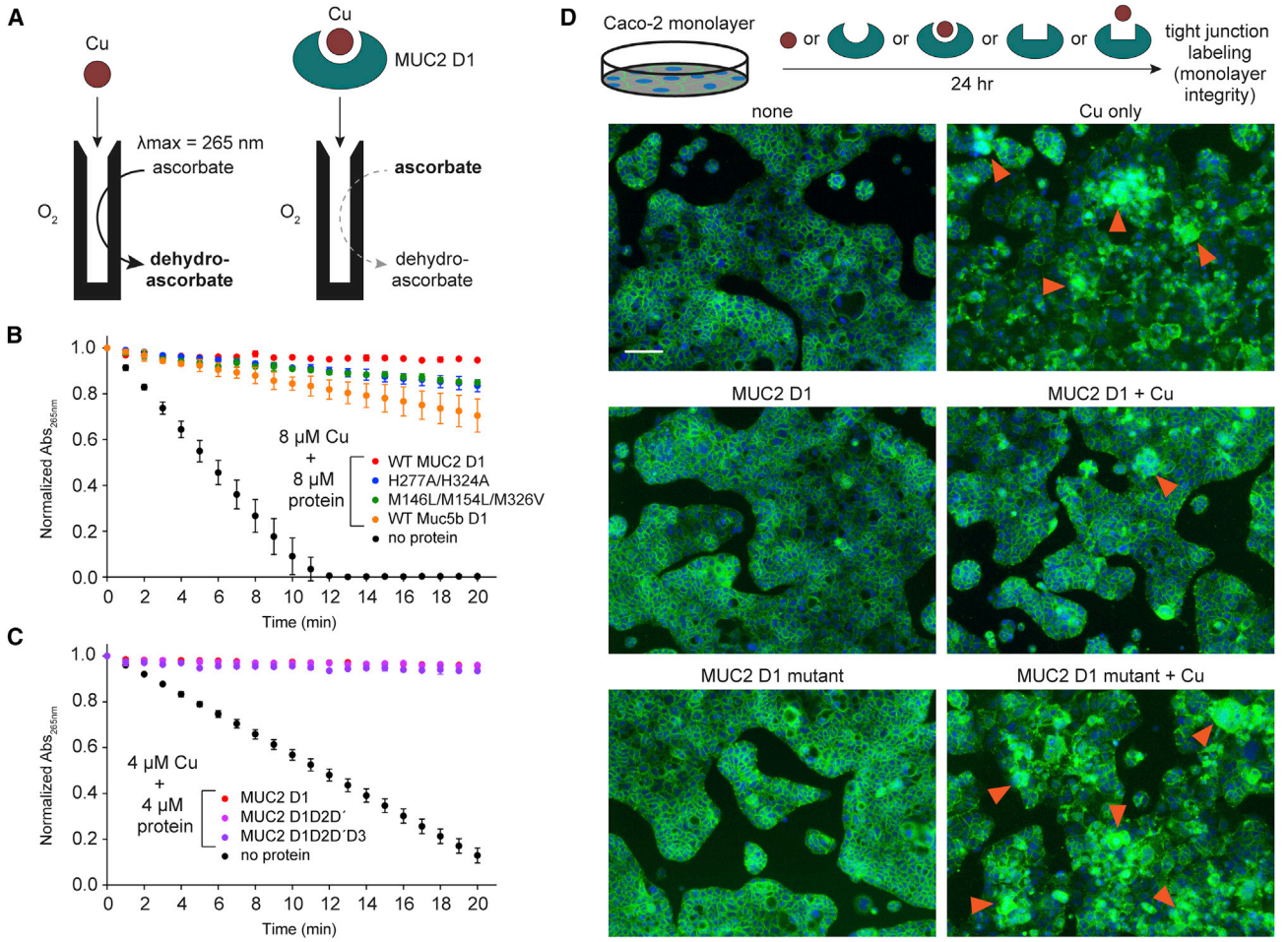

Figure 4. MUC2 D1 prevents the generation of reactive oxygen species and protects colon cells against toxic copper concentrations

(A) Ascorbate oxidation in aerobic solution was measured by the decrease in absorbance at 265 nm. Copper catalyzes ascorbate oxidation; binding of copper by MUC2 D1 inhibits this process.

(B) MUC2 D1 WT (red) prevented Cu^{2+}-driven ascorbate oxidation, whereas the H277A/H324A mutant (blue) and the triple methionine mutant (M146L/M154L/M326V) (green) decreased the rate of oxidation compared to Cu^{2+} alone (black). WT Muc5b D1 (orange) was less active than MUC2 D1 in preventing ascorbate oxidation. Copper and protein concentrations were 8 μM. Data are averages of two separate measurements for each protein variant, and errors are SD.

(C) Longer MUC2 segments prevented Cu^{2+}-driven ascorbate oxidation. Copper and protein concentrations were 4 μM. Lower concentrations of copper and protein were used in this experiment due to the high background absorbance of D1D2D′ and D1D2D′D3 at the measurement wavelength. Data are an average of two separate measurements for each protein variant, and errors are SD.

(D) Caco-2 colon cells were subjected to the indicated treatments in serum-free medium and then stained with DAPI (nuclei, blue) and labeled for E-cadherin (green). A network-like pattern of tight-junction labeling between closely packed cells indicates healthy cell monolayers, whereas uneven, patchy labeling (examples indicated by arrowheads) is characteristic of damaged monolayers. Cultures treated with a high copper concentration (250 μM) in the presence of equimolar wild-type MUC2 D1, but not of a H324A/M326V mutant, retained a healthy appearance.

Images presented are from a representative of three separate experiments, each conducted on two biological replicates. Scale bar is 100 μm.

that MUC2 D1 stabilizes Cu^{1+} in the presence of oxygen in a manner that prevents accumulation of ROS.

Based on this finding, we hypothesized that MUC2 might protect intestinal cells from toxic copper concentrations. E-cadherin labeling of Caco-2 human colorectal adenocarcinoma cells, which do not express significant MUC2 (van Klinken et al., 1996), was used to report on the integrity of cell-cell contact sites and the health of the monolayer. Addition of 250 μM Cu^{2+} in serum-free medium resulted in dramatic loss of the organized networks of E-cadherin seen in control cultures (Figure 4D). Supplying 250 μM MUC2 D1 together with 250 μM Cu^{2+} almost completely reversed this phenomenon, but a D1 mutant with perturbed copper binding sites, H324A/M326V, was unable to protect (Figure 4D).

MUC2 permits copper uptake into cells

The ability of MUC2 D1 to neutralize the toxicity of excess copper led us to ask whether D1 completely sequesters extracellular copper, or rather permits copper uptake for beneficial physiological processes. To address this question, we investigated whether nutritional levels of copper, i.e., sufficient copper to maintain basic cellular metabolic functions, supplied with D1 can be taken

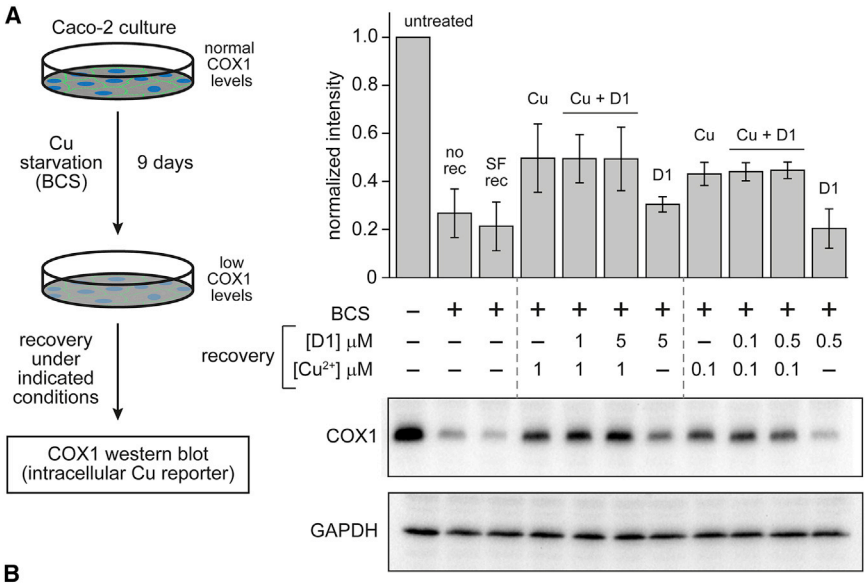

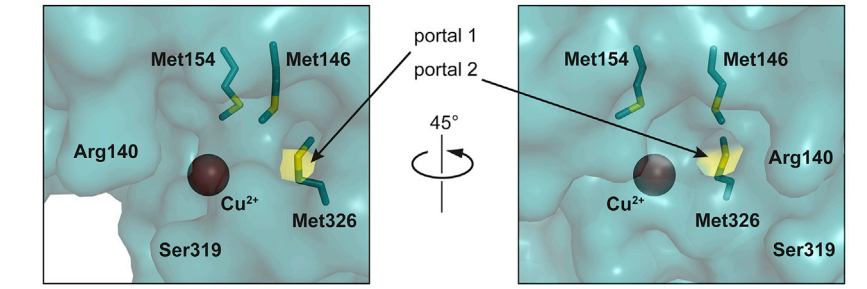

Figure 5. MUC2 D1 can release copper to cells

(A) Supplying copper bound to MUC2 D1 restored COX1 levels in copper-starved Caco-2 cells as detected by western blot. "SF rec" (Serum Free recovery) indicates that only serum-free medium was supplied during the recovery period, whereas the "no rec" (no recovery) sample was harvested without recovery. Dashed gray lines separate sets of samples with higher and lower copper and D1 concentrations during recovery. A representative blot is shown, and the bar graph presents averages of three independent experiments. Errors are SD.

(B) Met326 is exposed to the exterior of the protein through two small portals. A surface representation of the Cu^{2+}-bound MUC2 D1 crystal structure is shown with methionine sulfur atoms colored yellow.

See also Figure S6.

up by copper-starved cells. Caco-2 cells were deprived of copper by growth in the presence of the Cu^{1+} chelator bathocuproine disulfonate (BCS) until a severe drop was seen in the level of the mitochondrial electron transport chain component cytochrome *c* oxidase subunit 1 (COX1), which requires copper for function (Getz et al., 2011). Limited amounts of copper, 0.1 or 1 μM, were then re-supplied as Cu^{2+}, either alone or in the presence of stoichiometric or excess MUC2 D1, and the recovery of COX1 levels was monitored. Recovery proceeded even with a 5-fold excess of D1 over copper, in a concentration range substantially over the dissociation constant, suggesting that D1 can release needed copper to cells (Figures 5A and S6). It should be noted that Cu^{2+} added to the medium may become reduced to Cu^{1+}, consistent with the efficacy of the Cu^{1+} chelator BCS in inducing copper starvation. Hinting at a mechanism for Cu^{1+} transfer, the Cu^{1+} ligands in MUC2 D1, though buried within the protein, are adjacent to a small interior tunnel with two portals at the protein surface (Figure 5B). Together these findings show that MUC2 guards cells from the toxicity of excess copper without blocking supply of the low levels of copper required to maintain physiological processes.

DISCUSSION

Mucins are multifunctional molecules that promote mucosal health by restricting access of pathogens to the epithelial cell surface, storing factors that participate in innate immunity, and managing the microbiome (McGuckin et al., 2011; Johansson and Hansson, 2016; Chairatana and Nolan, 2017; Benam et al., 2018; Bankole et al., 2021). Moreover, secreted mucins were hypothesized to act not only as a protective barrier but also as regulators of small molecule access to membrane-embedded receptors and transporters (Strous and Dekker, 1992). However, investigating the molecular mechanisms of mucin function has long been limited by the lack of high-resolution mucin structures. Remarkably, a specific role for mucins in managing copper was revealed when structural information became available to inspire and inform the experiments reported in this work.

The studies presented here show that mucin D1 assemblies are specific for copper over a variety of other metals tested. Weak binding to zinc was also detected, but copper outcompeted zinc for binding to MUC2 D1, even when zinc was present in great molar excess (Figure S1C). The specialization of the mucin D1 assembly for copper binding contrasts with a separate, conserved calcium binding site present in all three D assemblies in the amino-terminal region of MUC2 (Javitt et al., 2020) and in the related blood clotting glycoprotein von Willebrand factor (Dong et al., 2019; Javitt and Fass, 2022). Unlike previous D-assembly crystal structures (Dong et al., 2019; Javitt et al., 2019), the Cu^{2+}-bound MUC2 D1 structure lacked calcium, probably due to the crystallization conditions. However, it is likely that calcium was bound to the purified MUC2 D1 in solution, as Ca^{2+} addition alone had no effect on the protein in MST (Figure S1B) or DSF (Figure S4A) experiments. Cu^{2+} addition, in contrast, showed a strong effect on thermophoresis and thermal stability in these experiments, indicating that the purified protein was in the apo state for this element. In particular, a single thermal unfolding transition was found for MUC2 D1

without addition of Cu^{2+} (Figure S4A), which shifted completely to a higher temperature in the presence of Cu^{2+}, providing support for the homogeneity of the protein prior to and following stoichiometric Cu^{2+} addition.

In contrast to Ca^{2+}, which is bound locally within the VWD domains of the D assemblies, Cu^{2+} is bound at the interface between three separate domains in D1: VWD1, C8-1, and TIL-1 (Figure 2A). One Cu^{2+} ligand is provided by each of these domains, and the fourth ligand is supplied by the flexible region at the amino terminus of the protein, just upstream of the VWD1 domain (Figure 2B). The distinct Cu^{2+} coordination geometry of MUC2 D1 compared to other copper-binding proteins with similar ligands (Figure S2) may reflect the independent evolutionary origin of copper binding by mucins, as well as mechanistic requirements for transfer of the bound Cu^{2+} to the Cu^{1+} site upon reduction. At the Cu^{1+} site, the amino terminus and C8-1 do not participate, and the Cu^{1+} ligands are provided by the VWD1 and TIL-1 domains. The binding of copper between multiple domains suggests that affinity for copper is tunable by factors or events, such as supramolecular assembly (Javitt et al., 2020) or interactions with other proteins, that may affect the relative orientations of those domains. Indeed, the TIL-1 and E-1 domains are flexible relative to the VWD1 and C8-1 domains, affecting the availability of the key copper ligand H324 (Figure 2C). Thus, in addition to the potential exit of Cu^{1+} through the portals seen in the MUC2 D1 crystal structure (Figure 5B), copper in either oxidation state may in principle be released by changes in the relative orientations of the domains constituting the D1 assembly. The conformational changes that mucins undergo during trafficking, storage, secretion, and extracellular function can now be studied with an eye toward their effect on copper coordination and release.

With detailed structural and biochemical information available, a physiological role for copper binding by mucins can be considered. Just as mucins themselves have many functions, copper binding by mucins may serve various purposes. MUC2 is expressed at high levels in all parts of the intestine, including both aerobic and anaerobic environments and regions with different digestive, absorptive, and excretive roles (Audie et al., 1993; Paone and Cani, 2020). In addition to protecting the intestines and other mucosal surfaces against copper toxicity, copper binding by mucins may facilitate the conversion of dietary copper (largely Cu^{2+}) to the form transported across the enterocyte membrane (thought to be Cu^{1+}). Notably, the high citrate concentration in the crystallization buffer did not prevent copper binding by MUC2 D1, indicating that the mucin competes well with organic acids that solubilize copper in the diet (Wapnir, 1998). The mechanisms by which dietary copper passes from the lumen of the digestive tract into enterocytes are debated (Zimnicka et al., 2007; Nose et al., 2010; Pierson et al., 2019). Hypothetically, MUC2 may interface structurally or functionally with the transmembrane copper transporter Ctr1, which uses methionines to coordinate Cu^{1+} in its pore (Ren et al., 2019), or with other proteins putatively involved in intestinal copper uptake (Nose et al., 2006). Mucins may also regulate copper delivery to commensal microorganisms or participate in nutritional immunity (Lopez and Skaar, 2018) by depriving pathogens of copper. MUC2 may cooperate with bile (Linder, 2020) for the safe excretion of excess copper. These activities need not be mutually exclusive. Further exploration of these various possibilities will help integrate mucins into models of physiological copper management (Shanbhag et al., 2021).

It is well known that copper is carefully regulated in biology. Transfer of copper within eukaryotic cells and in the bacterial periplasm is done by direct protein-protein contacts and ligand exchange rather than by release of copper into solution (Robinson and Winge, 2010; Nevitt et al., 2012). The players and mechanisms of copper chaperoning inside cells and in blood are relatively well understood (Nevitt et al., 2012; Linder, 2016; Magistrato et al., 2019), but how the body manages copper before it reaches those sites has been obscure. To date, one small gastrointestinal mucosal protein, TFF1, has been reported to bind copper using a flexible carboxy-terminal tail containing a cysteine and acidic residues (Tosco et al., 2010), but structural information on the binding mode is lacking. The lung and gastrointestinal mucosa are the largest, most important, and most vulnerable of exposed physiological surfaces, so it is reasonable that mechanisms would have evolved for restraining an essential but toxic element in these environments. The discovery that multiple gel-forming mucins are copper binding proteins, with an elaborate two-tiered site for distinct copper oxidation states in intestinal mucin (Figure 6), introduces intriguing new players into the field of copper regulation and utilization in the human body.

Limitations of the study

Our data clearly establish that conserved clusters of amino acids in gel-forming mucins preferentially bind copper and that the intestinal mucin MUC2 has a two-tiered site for binding of multiple copper oxidation states. The conservation of the copper-coordinating amino acids across animal species and the lack of variability in the human population suggest functional importance, but the physiological roles for copper binding by mucins remain to be established. Results presented here are consistent with several possibilities, including preventing the generation of damaging reactive oxygen species by blocking futile redox cycling. Moreover, MUC2 capturing of copper was shown not to interfere with copper uptake into cells, but a role in direct delivery of copper to cells is hypothetical at this point. A definitive demonstration of functional importance will require eliminating the MUC2 copper binding capability in a transgenic animal to determine the impact on copper metabolism and on commensal and pathogenic microorganisms. Additional mechanistic questions remain open, such as whether Cu^{1+} and Cu^{2+} can bind MUC2 simultaneously and what factors affect the kinetics of binding and release.

STAR★METHODS

Detailed methods are provided in the online version of this paper and include the following:

- KEY RESOURCES TABLE
- RESOURCE AVAILABILITY
  - Lead contact
  - Materials availability
  - Data and code availability

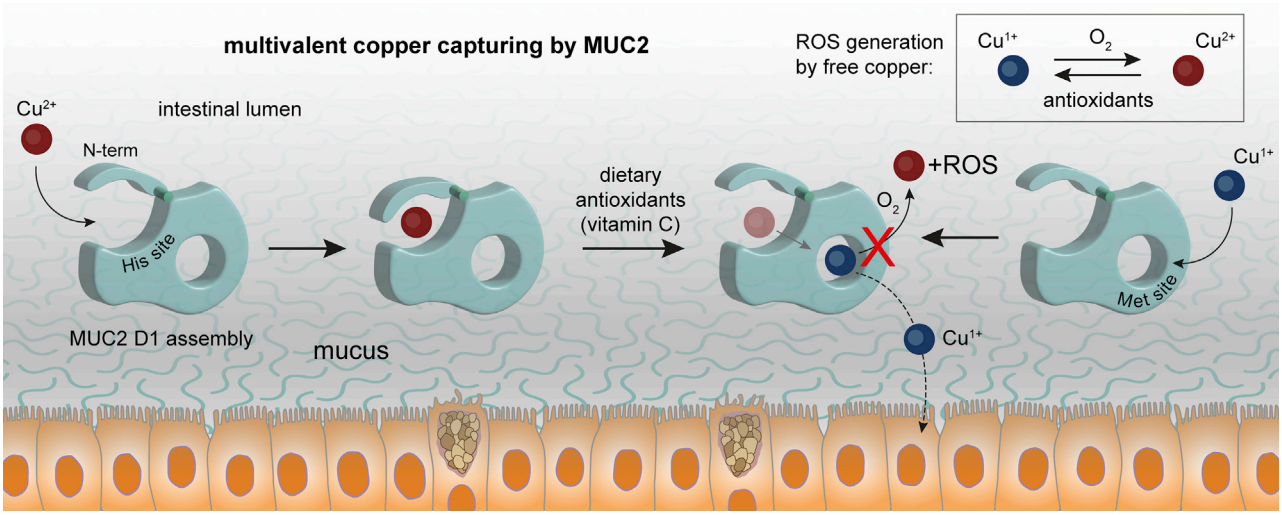

Figure 6. Summary of copper chaperoning by MUC2

A schematic illustration of the MUC2 two-tiered copper binding site, in which a histidine-rich site (His site) captures Cu^{2+} and a methionine-rich site (Met site) binds Cu^{1+}. MUC2-bound Cu^{2+} can be reduced to Cu^{1+} by vitamin C (ascorbate) or other dietary antioxidants. Bound Cu^{1+} is protected by MUC2 from oxidation in aerobic environments, but copper, putatively in the form of Cu^{1+}, can be released by MUC2 for nutritional delivery to cells (dashed arrow).

- EXPERIMENTAL MODEL AND SUBJECT DETAILS
  - Cell lines
  - Mice
- METHOD DETAILS
  - Protein production and purification
  - Crystallization and structure solution
  - Isothermal titration calorimetry (ITC)
  - Differential scanning fluorimetry (DSF)
  - Microscale thermophoresis (MST)
  - X-Ray absorption spectroscopy
  - Cu^{1+} quantification
  - Competition titrations and data fitting
  - Ascorbate oxidation assay
  - Cell toxicity assay
  - COX1 recovery assay
  - MUC2 western blotting
- QUANTIFICATION AND STATISTICAL ANALYSIS

SUPPLEMENTAL INFORMATION

Supplemental information can be found online at https://doi.org/10.1016/j.cell.2022.09.021.

ACKNOWLEDGMENTS

We thank Prof. Byung-Eun Kim for helpful suggestions. This work was supported by the Israel Science Foundation (2660/20), by the Minerva Foundation (136813), and by a research grant from the Center for Scientific Excellence at the Weizmann Institute of Science to D.F. Assays done by A.D.G. were developed with support from the US National Science Foundation CHE-1808710 to K.J.F. Funding from the U.S.-Israel Binational Science Foundation (ISF) (2021097) to D.F., K.J.F., and K.N.C. supported publication of this study.

AUTHOR CONTRIBUTIONS

D.F., K.J.F., and N.R. conceptualized and designed research. N.R., A.D.G., Y.F.-S., G.J., N.A.N., K.N.C., K.W.R., and D.F. carried out experiments. Y.F.-S. and T.I. provided methodology and expertise. N.R., A.D.G., K.W.R., K.N.C., S.F., D.G., and D.F. analyzed data. D.F. wrote the original manuscript draft, and D.F., K.J.F., and N.R. reviewed and edited the manuscript with input from all authors.

DECLARATION OF INTERESTS

The authors declare no competing interests.

Received: January 20, 2022
Revised: June 21, 2022
Accepted: September 9, 2022
Published: October 6, 2022

REFERENCES

Acevedo, K., Masaldan, S., Opazo, C.M., and Bush, A.I. (2019). Redox active metals in neurodegenerative diseases. J. Biol. Inorg. Chem. *24*, 1141–1157. https://doi.org/10.1007/s00775-019-01731-9.

Adams, P.D., Afonine, P.V., Bunkóczi, G., Chen, V.B., Davis, I.W., Echols, N., Headd, J.J., Hung, L.-W., Kapral, G.J., Grosse-Kunstleve, R.W., et al. (2010). PHENIX: a comprehensive Python-based system for macromolecular structure solution. Acta Crystallogr. D *66*, 213–221. https://doi.org/10.1107/S0907444909052925.

Audie, J.P., Janin, A., Porchet, N., Copin, M.C., Gosselin, B., and Aubert, J.P. (1993). Expression of human mucin genes in respiratory, digestive, and reproductive tracts ascertained by *in situ* hybridization. J. Histochem. Cytochem. *41*, 1479–1485. https://doi.org/10.1177/41.10.8245407.

Bankole, E., Read, E., Curtis, M.A., Neves, J.F., and Garnett, J.A. (2021). The relationship between mucins and ulcerative colitis: a systematic review. J. Clin. Med. *10*, 1935. https://doi.org/10.3390/jcm10091935.

Benam, K.H., Vladar, E.K., Janssen, W.J., and Evans, C.M. (2018). Mucociliary defense: emerging cellular, molecular, and animal models. Ann. Am. Thorac. Soc. *15*, S210–S215. https://doi.org/10.1513/AnnalsATS.201806-439AW.

Buettner, G.R., and Jurkiewicz, B.A. (1996). Catalytic metals, ascorbate and free radicals: combinations to avoid. Radiat. Res. *145*, 532. https://doi.org/10.2307/3579271.

Chacón, K.N., Mealman, T.D., McEvoy, M.M., and Blackburn, N.J. (2014). Tracking metal ions through a Cu/Ag efflux pump assigns the functional roles of the periplasmic proteins. Proc. Natl. Acad. Sci. USA *111*, 15373–15378. https://doi.org/10.1073/pnas.1411475111.

Chairatana, P., and Nolan, E.M. (2017). Defensins, lectins, mucins, and secretory immunoglobulin A: microbe-binding biomolecules that contribute to mucosal immunity in the human gut. Crit. Rev. Biochem. Mol. Biol. *52*, 45–56. https://doi.org/10.1080/10409238.2016.1243654.

DeLano, W.L. (2002). Pymol: An open-source molecular graphics tool. CCP4 Newsletter on Protein Crystallography *40*, 82–92.

DiNicolantonio, J.J., Mangan, D., and O'Keefe, J.H. (2018). Copper deficiency may be a leading cause of ischaemic heart disease. Open Heart *5*, e000784. https://doi.org/10.1136/openhrt-2018-000784.

Dong, X., Leksa, N.C., Chhabra, E.S., Arndt, J.W., Lu, Q., Knockenhauer, K.E., Peters, R.T., and Springer, T.A. (2019). The von Willebrand factor D'D3 assembly and structural principles for factor VIII binding and concatemer biogenesis. Blood *133*, 1523–1533. https://doi.org/10.1182/blood-2018-10-876300.

Emsley, P., Lohkamp, B., Scott, W.G., and Cowtan, K. (2010). Features and development of Coot. Acta Crystallogr. D *66*, 486–501. https://doi.org/10.1107/S0907444910007493.

Getz, J., Lin, D., and Medeiros, D.M. (2011). The cardiac copper chaperone proteins Sco1 and CCS are up-regulated, but Cox1 and Cox4 are down-regulated, by copper deficiency. Biol. Trace Elem. Res. *143*, 368–377. https://doi.org/10.1007/s12011-010-8858-z.

Hoffmann, W. (2021). Trefoil Factor Family (TFF) Peptides and their Different Roles in the Mucosal Innate Immune Defense and More: An Update. Curr Med Chem *28*, 7387–7399. https://doi.org/10.2174/0929867328666210215114140.

Ireland, S.M., and Martin, A.C.R. (2019). ZincBind– the database of zinc binding sites. Database 2019. baz006. https://doi.org/10.1093/database/baz006.

Karczewski, K.J., Francioli, L.C., Tiao, G., Cummings, B.B., Alfoldi, J., Wang, Q., Collins, R.L., Laricchia, K.M., Ganna, A., Birnbaum, D.P., et al. (2020). The mutational constraint spectrum quantified from variation in 141, 456 humans. Nature *581*, 434–443. https://doi.org/10.1038/s41586-020-2308-7.

Javitt, G., Calvo, M.L.G., Albert, L., Reznik, N., Ilani, T., Diskin, R., and Fass, D. (2019). Intestinal gel-forming mucins polymerize by disulfide-mediated dimerization of D3 domains. J. Mol. Biol. *431*, 3740–3752. https://doi.org/10.1016/j.jmb.2019.07.018.

Javitt, G., Khmelnitsky, L., Albert, L., Bigman, L.S., Elad, N., Morgenstern, D., Ilani, T., Levy, Y., Diskin, R., and Fass, D. (2020). Assembly Mechanism of Mucin and von Willebrand Factor Polymers. Cell *183*, 717–729.e16. https://doi.org/10.1016/j.cell.2020.09.021.

Javitt, G., and Fass, D. (2022). Helical self-assembly of a mucin segment suggests an evolutionary origin for von Willebrand factor tubules. Proc. Natl. Acad. Sci. USA *119*, e2116790119. https://doi.org/10.1073/pnas.2116790119.

Johansson, M.E.V., and Hansson, G.C. (2016). Immunological aspects of intestinal mucus and mucins. Nat. Rev. Immunol. *16*, 639–649. https://doi.org/10.1038/nri.2016.88.

Linder, M.C. (2016). Ceruloplasmin and other copper binding components of blood plasma and their functions: an update. Metallomics *8*, 887–905. https://doi.org/10.1039/c6mt00103c.

Linder, M.C. (2020). Copper Homeostasis in Mammals, with Emphasis on Secretion and Excretion. A Review. Int. J. Mol. Sci. *21*, 4932. https://doi.org/10.3390/ijms21144932.

Lopez, C.A., and Skaar, E.P. (2018). The impact of dietary transition metals on host-bacterial interactions. Cell Host Microbe *23*, 737–748. https://doi.org/10.1016/j.chom.2018.05.008.

Magistrato, A., Pavlin, M., Qasem, Z., and Ruthstein, S. (2019). Copper trafficking in eukaryotic systems: current knowledge from experimental and computational efforts. Curr. Opin. Struct. Biol. *58*, 26–33. https://doi.org/10.1016/j.sbi.2019.05.002.

Martin-Diaconescu, V., Chacón, K.N., Delgado-Jaime, M.U., Sokaras, D., Weng, T.-C., DeBeer, S., and Blackburn, N.J. (2016). Kβ Valence to core X-ray emission studies of Cu(I) binding proteins with mixed methionine-histidine coordination. Relevance to the reactivity of the M- and H-sites of peptidylglycine monooxygenase. Inorg. Chem. *55*, 3431–3439. https://doi.org/10.1021/acs.inorgchem.5b02842.

McGuckin, M.A., Lindén, S.K., Sutton, P., and Florin, T.H. (2011). Mucin dynamics and enteric pathogens. Nat. Rev. Microbiol. *9*, 265–278. https://doi.org/10.1038/nrmicro2538.

Nevitt, T., Ohrvik, H., and Thiele, D.J. (2012). Charting the travels of copper in eukaryotes from yeast to mammals. Biochim. Biophys. Acta *1823*, 1580–1593. https://doi.org/10.1016/j.bbamcr.2012.02.011.

Nilsson, H.E., Ambort, D., Bäckström, M., Thomsson, E., Koeck, P.J., Hansson, G.C., and Hebert, H. (2014). Intestinal MUC2 mucin supramolecular topology by packing and release resting on D3 domain assembly. J. Mol. Biol. *426*, 2567–2579. https://doi.org/10.1016/j.jmb.2014.04.027.

Nose, Y., Kim, B.-E., and Thiele, D.J. (2006). Ctr1 drives intestinal copper absorption and is essential for growth, iron metabolism, and neonatal cardiac function. Cell Metab *4*, 235–244. https://doi.org/10.1016/j.cmet.2006.08.009.

Nose, Y., Wood, L.K., Kim, B.-E., Prohaska, J.R., Fry, R.S., Spears, J.W., and Thiele, D.J. (2010). Ctr1 is an apical copper transporter in mammalian intestinal epithelial cells in vivo that is controlled at the level of protein stability. J. Biol. Chem. *285*, 32385–32392. https://doi.org/10.1074/jbc.M110.143826.

Padra, M., Benktader, J., Robinson, K., and Lindén, S. (2019). Carbohydrate-Dependent and Antimicrobial Peptide Defence Mechanisms Against *Helicobacter pylori* Infections. Molecular Mechanisms of Inflammation: Induction, Resolution and Escape by *Helicobacter pylori421* (Springer, Cham), pp. 179–207.

Paone, P., and Cani, P.D. (2020). Mucus barrier, mucins and gut microbiota: the expected slimy partners? Gut *69*, 2232–2243. https://doi.org/10.1136/gutjnl-2020-322260.

Pierson, H., Yang, H., and Lutsenko, S. (2019). Copper transport and disease: what can we learn from organoids? Ann. Rev. Nutr. *39*, 75–94. https://doi.org/10.1146/annurev-nutr-082018-124242.

Ren, F., Logeman, B.L., Zhang, X., Liu, Y., Thiele, D.J., and Yuan, P. (2019). X-ray structures of the high-affinity copper transporter Ctr1. Nat. Commun. *10*, 1386. https://doi.org/10.1038/s41467-019-09376-7.

Robinson, N.J., and Winge, D.R. (2010). Copper metallochaperones. Annu. Rev. Biochem. *79*, 537–562. https://doi.org/10.1146/annurev-biochem-030409-143539.

Rubino, J.T., and Franz, K.J. (2012). Coordination chemistry of copper proteins: how nature handles a toxic cargo for essential function. J. Inorg. Biochem. *107*, 129–143. https://doi.org/10.1016/j.jinorgbio.2011.11.024.

Schütte, A., Ermund, A., Becker-Pauly, C., Johansson, M.E.V., Rodriguez-Pineiro, A.M., Bäckhed, F., Müller, S., Lottaz, D., Bond, J.S., and Hansson, G.C. (2014). Microbial-induced meprin β cleavage in MUC2 mucin and a functional CFTR channel are required to release anchored small intestinal mucus. Proc. Natl. Acad. Sci. USA. *111*, 12396–12401. https://doi.org/10.1073/pnas.1407597111.

Shanbhag, V.C., Gudekar, N., Jasmer, K., Papageorgiou, C., Singh, K., and Petris, M.J. (2021). Copper metabolism as a unique vulnerability in cancer. Biochim. Biophy. Acta Mol. Cell. Res. *1868*, 118893. https://doi.org/10.1016/j.bbamcr.2020.118893.

Strous, G.J., and Dekker, J. (1992). Mucin-type glycoproteins. Crit. Rev. Biochem. Mol. Biol. *27*, 57–92. https://doi.org/10.3109/10409239209082559.

Tosco, A., Monti, M.C., Fontanella, B., Montefusco, S., D'Andrea, L., Ziaco, B., Baldantoni, D., Rio, M.C., and Marzullo, L. (2010). Copper binds the carboxy-terminus of trefoil protein 1 (TFF1), favoring its homodimerization and

motogenic activity. Cell. Mol. Life Sci. *67*, 1943–1955. https://doi.org/10.1007/s00018-010-0309-7.

Tottey, S., Waldron, K.J., Firbank, S.J., Reale, B., Bessant, C., Sato, K., Cheek, T.R., Gray, J., Banfield, M.J., Dennison, C., and Robinson, N.J. (2008). Protein-folding location can regulate manganese-binding versus copper- or zinc-binding. Nature *455*, 1138–1142. https://doi.org/10.1038/nature07340.

Trapaidze, A., Hureau, C., Bal, W., Winterhalter, M., and Faller, P. (2012). Thermodynamic study of Cu^{2+} binding to the DAHK and GHK peptides by isothermal titration calorimetry (ITC) with the weaker competitor glycine. J. Biol. Inorg. Chem. *17*, 37–47. https://doi.org/10.1007/s00775-011-0824-5.

van Klinken, B.J.W., Oussoren, E., Weenink, J.J., Strous, G.J., Büller, H.A., Dekker, J., and Einerhand, A.W.C. (1996). The human intestinal cell lines Caco-2 and LS174T as models to study cell-type specific mucin expression. Glycoconj. J. *13*, 757–768. https://doi.org/10.1007/BF00702340.

Wapnir, R.A. (1998). Copper absorption and bioavailability. Am. J. Clin. Nutr. *67*, 1054S–1060S. https://doi.org/10.1093/ajcn/67.5.1054S.

Xiao, Z., Gottschlich, L., van der Meulen, R., Udagedara, S.R., and Wedd, A.G. (2013). Evaluation of quantitative probes for weaker Cu(I) binding sites completes a set of four capable of detecting Cu(I) affinities from nanomolar to attomolar. Metallomics *5*, 501. https://doi.org/10.1039/c3mt00032j.

Young, T.R., and Xiao, Z. (2021). Principles and practice of determining metal-protein affinities. Biochem. J. *478*, 1085–1116. https://doi.org/10.1042/BCJ20200838.

Zimnicka, A.M., Maryon, E.B., and Kaplan, J.H. (2007). Human copper transporter hCTR1 mediates basolateral uptake of copper into enterocytes: implications for copper homeostasis. J. Biol. Chem. *282*, 26471–26480. https://doi.org/10.1074/jbc.M702653200.

STAR★METHODS

KEY RESOURCES TABLE

REAGENT or RESOURCE	SOURCE	IDENTIFIER
Antibodies		
anti MTCO1	Abcam	Cat # Ab14705
anti E-cadherin	Abcam	Cat # Ab231303
Goat anti mouse-HRP	Jackson ImmunoResearch	Cat # 115-035-062
Goat anti mouse-Alexa Fluor 488	Abcam	Cat # Ab150113
rabbit anti MUC2 D1 polyclonal	produced for this study	RRID:AB_2924251
Chemicals, peptides, and recombinant proteins		
kifunensine	Cayman Chemicals	Cat # 10,009,437
EndoH	New England Biolabs	Cat # P0702S
L-ascorbic acid	Sigma	Cat # A0278
Quercitin	Sigma	Cat # Q4951
pcDNA3.1-MUC2 D1	this study	Addgene ID 181812
pcDNA3.1-MUC2 D1 with cleavable His tag	this study	Addgene ID 181813
pcDNA3.1-MUC2 D1D2D′ with cleavable His tag	this study	Addgene ID 187993
pcDNA3.1-MUC2 D1D2D′D3 with cleavable His tag	this study	Addgene ID 187994
pcDNA3.1-Muc5b D1 (murine) with cleavable His tag	this study	Addgene ID 181814
Tobacco Etch Virus Protease	produced in house	N/A
Deposited Data		
MUC2 D1 with bound Cu^{2+}	PDB	PDB:7PRL
Experimental models: Cell lines		
Caco-2	Laboratory of Prof. Benjamin Geiger	ATCC HTB-37
Software and algorithms		
Pymol	DeLano (2002)	https://pymol.org/2/
Coot	Elmsley et al. (2010)	https://www2.mrc-lmb.cam.ac.uk/personal/pemsley/coot/
Phenix	Adams et al. (2010)	https://www.phenix-online.org/
EXAFSPAK	George GN.	https://www-ssrl.slac.stanford.edu/exafspak.html
EXCURVE	Tomic S.	https://software.pan-data.eu/software/85/dl-excurv-formerly-excurve

RESOURCE AVAILABILITY

Lead contact

Requests for further information or reagents may be addressed to the lead contact, Deborah Fass (deborah.fass@weizmann.ac.il).

Materials availability

The primary plasmids used in this study were deposited to Addgene (identifiers: #181812, #181813, #181814, #187993, and #187994).

Data and code availability

Coordinates and structure factors for MUC2 D1 bound to Cu^{2+} have been deposited in the Protein Data Bank (PDB: 7PRL). Other data reported in this paper will be shared by the lead contact upon request. This paper does not report original code.

EXPERIMENTAL MODEL AND SUBJECT DETAILS

Cell lines

The human colon epithelial cell line Caco-2 were obtained from the laboratory of Prof. Benjamin Geiger (Weizmann Institute of Science) and grown in DMEM (Gibco, Thermo Fisher Scientific) supplemented with 10% fetal bovine serum, L-glutamine, and Pen-Strep (Biological Industries). Caco-2 cells were confirmed to be negative for mycoplasma. The human colon epithelial cell line LS174T was purchased from Sigma and grown in MEM (Sigma) supplemented with 10% fetal bovine serum, L-glutamine, and Pen-Strep (Biological Industries).

Mice

Wild-type strain C57BL mice, male, age 10 weeks, were obtained from a colony housed in the Weizmann Institute mice facility for experiments approved by the institutional animal care and use committee (IACUC) of the Weizmann Institute of Science, approval number 01280121-2.

METHOD DETAILS

Protein production and purification

The MUC2 D1 coding sequence (NCBI reference sequence NP_002448.4, amino acids 21–389) was cloned into the pCDNA3.1 vector following the signal sequence of the enzyme QSOX1. A His_6 tag was appended to the carboxy terminus. The plasmid was transiently transfected into HEK293F cells (Thermo Fisher Scientific) using the PEI Max reagent (Polysciences Inc.) with a 1:3 ratio (w/w) of DNA to PEI at a concentration of 1 million cells per mL. Cells were maintained in FreeStyle 293 medium (Thermo Fisher Scientific). To facilitate subsequent crystallization, 5 μM kifunensine (Cayman Chemical) was added at the time of transfection to obtain protein containing high-mannose, EndoH-cleavable glycans. Six days after transfection, cells were removed from the cultures by centrifugation for 10 min at 500xg. The culture medium was then further clarified by centrifugation for 30 min at 9500xg and filtration through a 0.45 μm pore-size membrane. The D1 assembly was purified from the medium by nickel-nitrilotriacetic acid (Ni-NTA) chromatography. Purified protein was exchanged into 25 mM 4-(2-hydroxyethyl)-1-piperazineethanesulfonic acid (HEPES), pH 7.5, 250 mM NaCl and concentrated to 10 mg/mL (240 μM). Protein concentration was determined by diluting an aliquot with 6 M guanidinium chloride in 20 mM sodium phosphate buffer, pH 7 and measuring absorbance at 280 nm against a blank containing the same volumes of guanidinium solution and buffer solution lacking protein (ε_{280nm} for MUC2 D1 = 43,245 M^{-1} cm^{-1}). EndoH (500 units) was added to 400 μL D1 and incubated overnight at room temperature before crystallization.

For experiments aside from crystallization, the MUC2 D1 expression construct was modified to contain a His_6 tag and tobacco etch virus (TEV) cleavage site following the signal sequence, and the His_6 tag at the carboxy terminus was eliminated. Protein was produced without kifunensine. After Ni-NTA purification, protein was subjected to cleavage with TEV protease containing a His_6 tag. The cleaved amino terminal tag and the TEV protease were subsequently removed using Ni-NTA beads. The protein was concentrated in 10 mM 3-(*N*-morpholino)propanesulfonic acid (MOPS) buffer, pH 7.0, 100 mM NaCl. Glycerol was added to 10%, and aliquots were stored at −80°C until use. An expression plasmid for Muc5b D1 (UniProt E9Q5I3 amino acids 50–426) was prepared with a TEV cleavage site followed by a His_6 tag at the carboxy terminus. Muc5b D1 was produced and purified as for MUC2 D1, subjected to TEV cleavage, and quantified as described above (ε_{280nm} for Muc5b D1 including the remaining segment of the TEV site = 50,360 M^{-1} cm^{-1}). Longer constructs of MUC2, namely D1D2D′ (amino acids 21–858) and D1D2D′D3 (amino acids 21–1259), were produced and purified as for MUC2 D1, subjected to TEV cleavage, and quantified as described above (ε_{280nm} for MUC2 D1D2D′ = 102,710 M^{-1} cm^{-1} and for MUC2 D1D2D′D3 = 167,760 M^{-1} cm^{-1}).

Crystallization and structure solution

The MUC2 D1 assembly containing a carboxy-terminal His_6 tag was crystallized using the hanging drop method over a well solution containing 30 mM $MgCl_2$, 8% polyethylene glycol 3350, 100 mM citrate buffer, pH 5.4, and 10% glycerol. The protein stock solution for crystallization was supplemented with 480 μM copper sulfate. Drops were prepared by mixing 2 μL protein with 1 μL well solution. Data-quality crystals grew slowly over the course of a few months. About 10 min prior to flash freezing, crystals were transferred to a solution containing all components of the well except that the glycerol concentration was increased to 20%. For reduction of Cu^{2+}, 5 mM ascorbic acid (Sigma) was included in this soak solution. Data were collected at the European Synchrotron Radiation Facility (ESRF) beamline ID23-1 at 100 K. The wavelength was 14.2 keV (0.8731 Å). Initial phases were provided by molecular replacement using the D1 assembly from the MUC2 amino-terminus cryo-EM structure (Javitt et al., 2020), and the structure model was improved by cycles of rebuilding using Coot (Elmsley et al., 2010) and refinement using Phenix (Adams et al., 2010). No Ramachandran outliers were present in the refined structure model, and 95.5% of the amino acids were in favored regions of Ramachandran space. Though the D1 assembly was previously seen to bind calcium in the cryo-EM structure (Javitt et al., 2020), no calcium was detected in the D1 crystal structure, most likely due to the high concentration of citrate in the crystallization buffer.

Isothermal titration calorimetry (ITC)

The use of glycine as a competitor for copper to enable accurate ITC measurements of high-affinity protein-copper interaction was based on published studies (Trapaidze et al., 2012). MUC2 D1 was dialyzed against 20 mM HEPES buffer, pH 7.4, containing 150 mM NaCl and 2, 10, or 30 mM glycine, or against HEPES buffer, pH 6.8, 150 mM NaCl, and 4 mM glycine. After dialysis, protein was diluted to a final concentration of 50 μM. $CuSO_4$ was prepared at 500 μM in the same dialysis buffer as the corresponding protein. Experiments were conducted at 25°C on a Malvern Micro-Cal PEAQ-ITC system starting with a single 0.4 μL injection of Cu^{2+} solution into protein solution, followed by 18 2-μL injections, with 150 s spacing between each injection and continuous stirring at 750 rpm. For each glycine concentration, a blank run titrating the Cu^{2+} into buffer was done and subtracted accordingly. The titration data were analyzed using software provided by the manufacturer to obtain the apparent K_D and other parameters. Conditional K_D values were derived according to published methods (Trapaidze et al., 2012).

For the set of measurements performed at pH 7.4, substoichiometric Cu^{2+} binding was observed, with Cu^{2+}:protein ratios of ~0.54:1. Measurements subsequently performed at pH 6.8 yielded Cu^{2+}:protein ratios of ~0.85:1. (Table 2). The reason for deviation from the expected 1:1 ratio is as yet unexplained. X-ray fluorescence counts at the copper edge showed that purified MUC2 D1 was not pre-loaded with Cu^{2+}, and measurements after addition of Cu^{2+} suggested stoichiometric binding. None of the other experiments performed (*i.e.*, crystallography, BCA colorimetric assays, or DSF) suggested either a fraction of copper pre-loaded protein or copper binding-incompetent protein. Protein concentrations were determined for ITC and EXAFS experiments using the same method and were done with care, such that it is unlikely that large errors in protein concentration determination explain the ITC results.

Differential scanning fluorimetry (DSF)

To compare thermal stabilization upon Cu binding by WT MUC2 segments and mutants, as well as by Muc5b, DSF was performed using a Prometheus NT.48 (NanoTemper) instrument. Proteins were used at a concentration of 5, 7.5, or 12 μM, as indicated in the figure legends. All metals were supplied at a 1:1 M ratio to protein. When present, ascorbic acid was added at a 20:1 M ratio to protein. Buffer was either 50 mM 2-(N-morpholino)ethanesulfonic acid (MES) buffer, pH 5.7, 100 mM NaCl, 0.05% Tween 20 or 50 mM MOPS buffer, pH 7.0, 100 mM NaCl, 0.05% Tween 20. Metals were supplied as: Cu, copper sulfate; Zn, zinc chloride; Ca, calcium chloride; Co, cobalt chloride; Ni, nickel sulfate; Fe, iron sulfate; Mn, manganese chloride; Hg, mercury chloride; Cd, cadmium acetate, Pb, lead chloride; As, sodium arsenite. Samples were heated from 25°C to 95°C at 1°C/min. Tryptophan and tyrosine fluorescence was monitored by recording the 350/330 nm emission ratio after excitation at 280 nm.

Microscale thermophoresis (MST)

MUC2 D1 was used at a concentration of 500 nM in 50 mM MOPS buffer, pH 7.0, 100 mM NaCl, 0.05% Tween 20. Protein was incubated with 16 serial dilutions of metal in the range of 50 μM to 1.5 nM for 10 min and centrifuged at 20,000xg for 10 min at 4°C. Tryptophan and tyrosine fluorescence was monitored and recorded using a Monolith Label-Free instrument (NanoTemper). Thermophoresis was analyzed at 70% LED and 20% infrared laser intensity for all samples. Initial fluorescence was equal in all capillaries before thermophoresis measurements. MST to analyze copper binding by Muc5b was performed in the same manner.

X-Ray absorption spectroscopy

A solution of 800 μM MUC2 D1 in 50 mM MES buffer, pH 5.7, 100 mM NaCl was incubated with 0.8:1 equiv of $CuSO_4$ via syringe pump to ensure no excess metal was present, then was split into two samples. One sample was treated with excess ascorbate to ensure the cuprous form of the metalloprotein, and both samples were measured as an aqueous glass in 20% ethylene glycol at 10 K. Cu K-edge (8.9 keV) extended X-ray absorption fine structure (EXAFS) and X-ray absorption edge data were collected at the Stanford Synchrotron Radiation Lightsource on beamline 7–3 with an Si 220 monochromator, in fluorescence mode using a high-count rate Canberra 30-element Ge array detector. A Ni filter and a Soller slit were placed in line with the detector to attenuate the elastic scatter peak. For energy calibration, a Cu foil was placed between the second and third ionization chambers. In the case of the Cu^{2+}-loaded sample, scans were taken from fresh surfaces of the sample window and their edges compared to ensure no photoreduction occurred, with a shutter in place in between scan points. Six scans of a buffer blank were averaged and subtracted from the raw data to produce a flat pre-edge and remove any residual Ni fluorescence. Data reduction and background subtraction were done using the EXAFSPAK suite, and the data were inspected for dropouts and glitches before averaging. The EXCURVE program was used for spectral simulations.

Cu^{1+} quantification

Samples of 60 μM MUC2 D1 were prepared in 50 mM MES buffer, pH 5.7, 100 mM NaCl. Where indicated, $CuSO_4$ was supplied at a concentration of 60 μM and, subsequently, ascorbic acid or quercetin was added to a concentration of 1.2 mM. Following a 5-min incubation, samples were exchanged into 50 mM MES buffer, pH 5.7, 100 mM NaCl using Zeba Spin Desalting Columns 7K MWCO (size exclusion) (Thermo Fisher Scientific) to remove ascorbic acid or quercetin, when present, and any copper not bound to protein. After desalting, samples were diluted by a factor of three (*i.e.*, to 20 μM MUC2 D1) into the same buffer containing bicinchoninic acid (BCA) (final BCA concentration 1 mM). Absorbance was measured at 562 nm, and data were converted to Cu^{1+} concentration using an extinction coefficient of 7,900 $M^{-1}cm^{-1}$ for the Cu^{1+}-$(BCA)_2$ complex (Young and Xiao, 2021). For the Zn^{2+} competition assay,

protein was first incubated for 10 min with Zn^{2+} (concentration ratios are indicated in Figure S1C). Subsequently, Cu^{2+} was added, and the buffer was exchanged using the spin columns described above. Ascorbic acid was added to the eluate to reduce any protein-bound Cu^{2+} obtained, and BCA was used to quantify the resulting Cu^{1+}.

Competition titrations and data fitting

UV/vis absorption spectra were recorded in a 1-cm quartz cuvette on an SI Photonics model 420 fiber optic CCD array spectrophotometer located inside a Siemens MBraun glove box under inert nitrogen atmosphere. Cu^{1+} stock solutions were prepared by dissolving $Cu(CH_3CN)_4PF_6$ in anhydrous acetonitrile and subsequently standardized using the chromophoric ligand BCS. The apparent affinity constants for Cu^{1+} of WT MUC2 D1 and various mutants were determined by competition titrations with colorimetric ligands (L) by using BCA as L in 50 mM MOPS buffer with 150 mM NaCl, pH 7.0, or ferrozine (Fz) or BCA as L in 50 mM MES buffer with 150 mM NaCl, pH 5.7 (Xiao et al., 2013; Young and Xiao, 2021). Aliquots of 10 mM L stock were titrated into solutions containing 50 μM protein and 25 μM $Cu(CH_3CN)_4PF_6$ (for L = BCA) or 55 μM protein and 50 μM $Cu(CH_3CN)_4PF_6$ (for L = Fz) to establish the exchange equilibrium expressed by Equations 1 and 2. Formation constants of 1.6×10^{17} and 1.3×10^{15} were used for Cu complexes with BCA and Fz, respectively (Xiao et al., 2013). The concentration of $[Cu(BCA)_2]^{3-}$ complex was calculated from its absorbance at 562 nm (ε = 7,900 $M^{-1}cm^{-1}$). The concentration of $[Cu(Fz)_2]^{3-}$ complex was calculated from its absorbance at 470 nm (ε = 4,320 $M^{-1}cm^{-1}$) (Xiao et al., 2013). Calculations of the other species present in solution were calculated from mass-balance equations. Data plotted as [L] vs. $[Cu(L)_2]$ were fit to Equation 3 using GraphPad Prism software to obtain $K_{exchange}$, where $K_{exchange}$ is designated as K, total [Cu] as M, total [MUC2 D1] as P, [L] as y, and $[Cu(L)_2]$ as x

$$PCu + 2\,L \rightarrow P + Cu(L)2 \tag{1}$$

$$K_{exchange} = \frac{[P]Cu(L)_2]}{[PCu][L]^2} = \frac{K_{Cu(L)_2}}{K_{PCu}^{app}} \tag{2}$$

$$y = \frac{-\sqrt{\left(-KM^2x + KMPx + 2KMx^2 - KPx^2 - Kx^3\right)} + 2KMx - 2Kx^2}{KM - Kx} \tag{3}$$

Ascorbate oxidation assay

Absorbance was recorded in 1-cm quartz cuvettes on a nanophotometer np80 (Implen) spectrophotometer. Cu^{2+} stock solution was prepared by dissolving copper sulfate in ultrapure water. Freshly prepared L-ascorbic acid (Sigma A0278) was added at a final concentration of 120 μM to buffered 8-μM or 4-μM Cu^{2+}-protein solutions, as indicated in the figure for each experiment. Buffer was 50 mM MOPS, pH 7.0, 100 mM NaCl.

Cell toxicity assay

Caco-2 cells were passaged in DMEM containing 10% fetal bovine serum (FBS), penicillin/streptomycin, and L-glutamine. Cells were seeded at density of 25,000 cells/well in a 96-well plate, 48 h prior to experiment. To initiate toxicity, cells were washed once with PBS, and additives for testing were supplied in serum-free medium. Proteins (wild-type or H324A/M326V MUC2 D1) and copper sulfate were supplied at 250 μM final concentrations. After 24 h, cells were washed with PBS and fixed with 4% paraformaldehyde. After blocking with BSA, cells were labeled with anti-E-cadherin antibody ab231303, 1:100 dilution) for 1 h at room temperature, followed by an Alexa 488 conjugated secondary antibody. Images were taken using a Olympus IX51 microscope equipped with Olympus XM10 camera.

COX1 recovery assay

Caco-2 cells were passaged in DMEM containing 10% fetal bovine serum (FBS), Pen-Strep, and L-glutamine. For copper starvation, medium was supplemented with 500 μM BCS for 9 days. During passaging under copper starvation conditions, cells were plated in parallel in 6 cm dishes. To initiate recovery, cells were washed once with PBS, and additives for testing were supplied in serum-free medium. After a further 3 days, cells were harvested by trypsinization and pelleted. Cell lysates were separated by SDS-PAGE and analyzed for COX1 levels by western blot (Anti-MTCO1 #ab14705). Bands were quantified using ImageJ software and normalized to the untreated sample for each biological experimental replicate.

MUC2 western blotting

LS174T cells (6×10^6) were seeded on a 10-cm tissue culture plate in serum-free medium. Supernatant was collected after 4 days in culture. Supernatant was centrifuged at 500xg for 10 min and concentrated by a factor of 10 using a 30 kDa cut-off centrifugal concentrator. SDS-PAGE was performed using a volume of 20 μL per lane. For western blotting of mucus extractions from mice, 1 cm segments of duodenum, intestine, and colon were incubated each in 300 μL of 8 M urea in PBS supplemented with a protease

inhibitor cocktail for 1 h at room temperature. Liquid was collected from the samples using a pipette and centrifuged at 17,000xg for 10 min. SDS-PAGE was performed using 35 μL of the supernatant per lane. Western blot analysis was performed using a rabbit polyclonal antibody raised against the recombinant human MUC2 D1 assembly and used at 8 μg/mL final concentration.

QUANTIFICATION AND STATISTICAL ANALYSIS

Errors for biochemical and cell biological experiments are reported as SD, and the number of measurements for each experiment is indicted in the figure legends. Statistical validation performed on the deposited atomic coordinate model was done using Phenix and is reported in Table S1.

CellPress
OPEN ACCESS

Supplemental figures

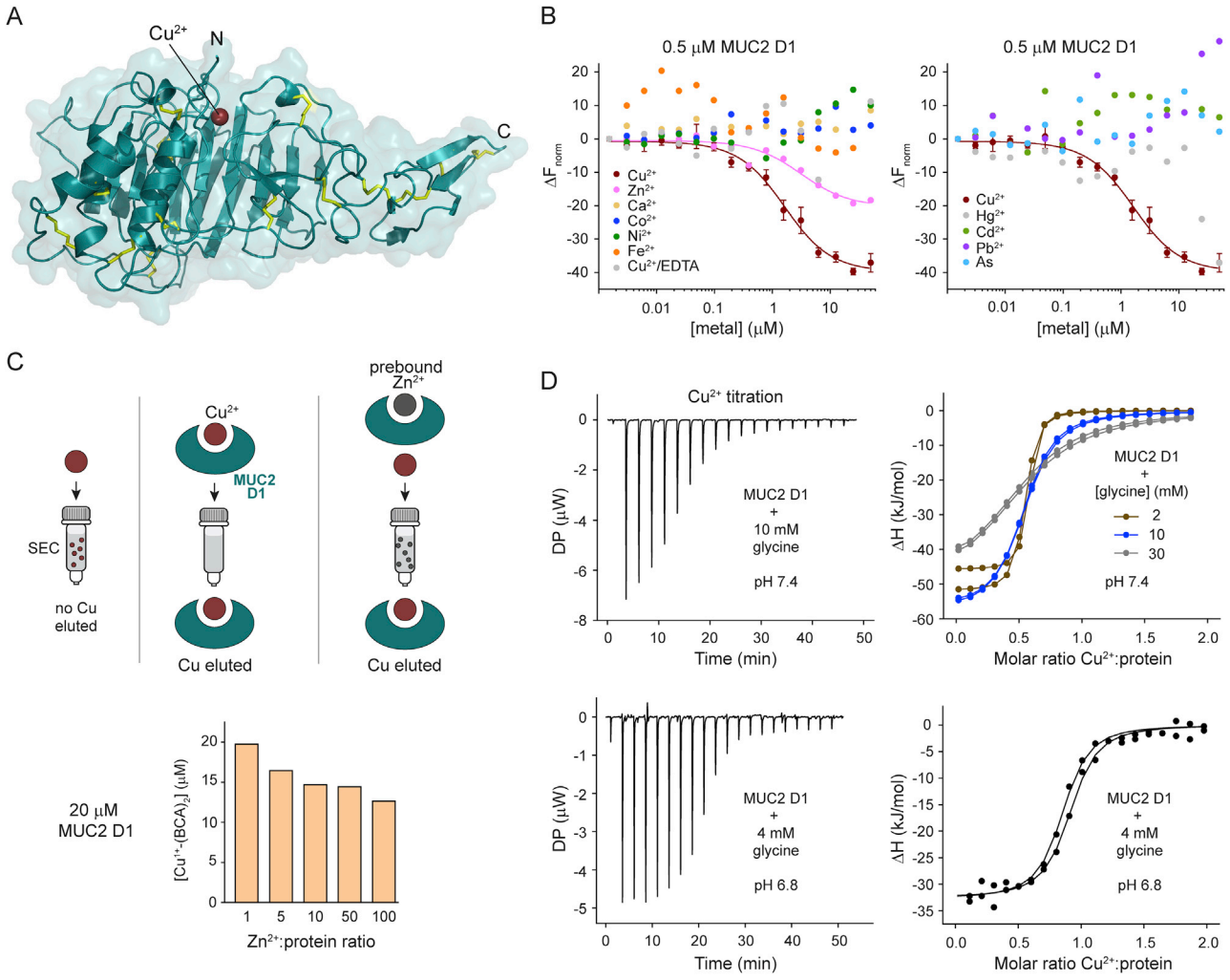

Figure S1. MUC2 specifically binds copper, related to Figure 2

(A) The crystal structure of the Cu^{2+}-bound MUC2 D1 assembly is shown rotated 90° around the x axis compared to Figure 2A. The Cu^{2+} binding site is near the upper surface of the protein in this view.

(B) MST demonstrated binding specificity of MUC2 D1 for Cu^{2+}. Only an upper limit on the binding constant for Cu^{2+} can be determined from this experiment due to the amount of protein required for the measurements (0.5 μM MUC2 D1). Cu^{2+} data are presented as the average of three measurements; other metals were measured once. Errors are SD.

(C) A preference for Cu^{2+} binding over Zn^{2+} was shown by pre-incubating MUC2 D1 with stoichiometric or excess Zn^{2+}, then adding Cu^{2+} at a 1:1 M ratio to protein and measuring the amount of copper that was recovered bound to protein as the eluate from a size exclusion spin column. Cu^{2+} that is prevented from binding due to the presence of Zn^{2+} would be retained in the spin column and not recovered in the eluate. Graph represents one measurement of each Zn concentration.

(D) ITC measurements in the presence of the competitive ligand glycine. On the left are representative titrations at the indicated pH values and glycine concentrations. On the right, binding isotherms are shown for two repetitions under each of the indicated conditions.

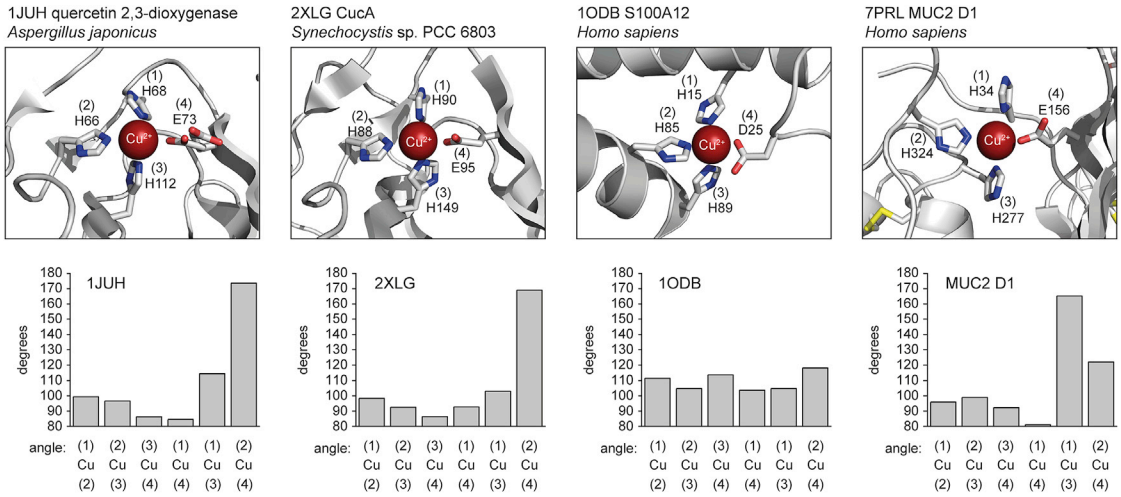

Figure S2. Comparison of copper binding ligand geometries, related to Figure 2

The top panels show examples of protein structures from the protein data bank (PDB) that coordinate copper with similar ligands as the Cu^{2+} site in MUC2 D1. Cu^{2+} coordinating side chains are shown as sticks and numbered according to the amino acid sequence of each protein. In addition, numbers in parentheses designate the coordinating residues counter-clockwise. The lower panels show the angle measured for each pair of coordinating atoms with the copper at the vertex. Quercetin 2,3-dioxygenase (1JUH) and CucA (2XLG) have similar sets of angles, and CucA exhibits some quercetin dioxygenase activity (Tottey et al., 2008). As indicated by all angles being close to 110°, the Cu^{2+} coordination geometry of S100A12 is approximately tetrahedral. The three histidines of MUC2 D1 are arranged roughly as three corners of a square plane (angles ~90°, ~90°, ~180°), while the glutamate is ~120° off the plane. This geometry is different from both 1JUH/2XLG and 1ODB.

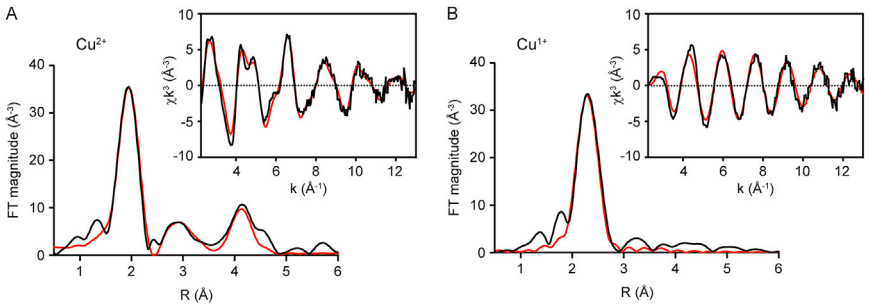

Figure S3. X-ray absorption data for Cu^{2+}- and Cu^{1+}-bound MUC2 D1, related to Figures 2 and 3.

Experimental (black) and simulated (red) Fourier transforms and EXAFS (inset) are displayed for Cu^{2+}-bound MUC2 D1 and Cu^{1+}-bound MUC2 D1 obtained by treating the Cu^{2+}-bound protein with ascorbate.

(A) An average Cu^{2+}–N bond distance of 2.018 Å and Debye Waller (DW) factor of 0.003 $Å^2$ were measured for the three His ligands, indicating a stable binding site. The Cu^{2+}–N/O bond distance determined by EXAFS, corresponding to the glutamate ligand, was best fit to 1.886 Å.

(B) An average Cu^{1+}–S bond length of 2.317 Å and DW of 0.011 $Å^2$ was calculated for methionine coordination of the reduced copper.

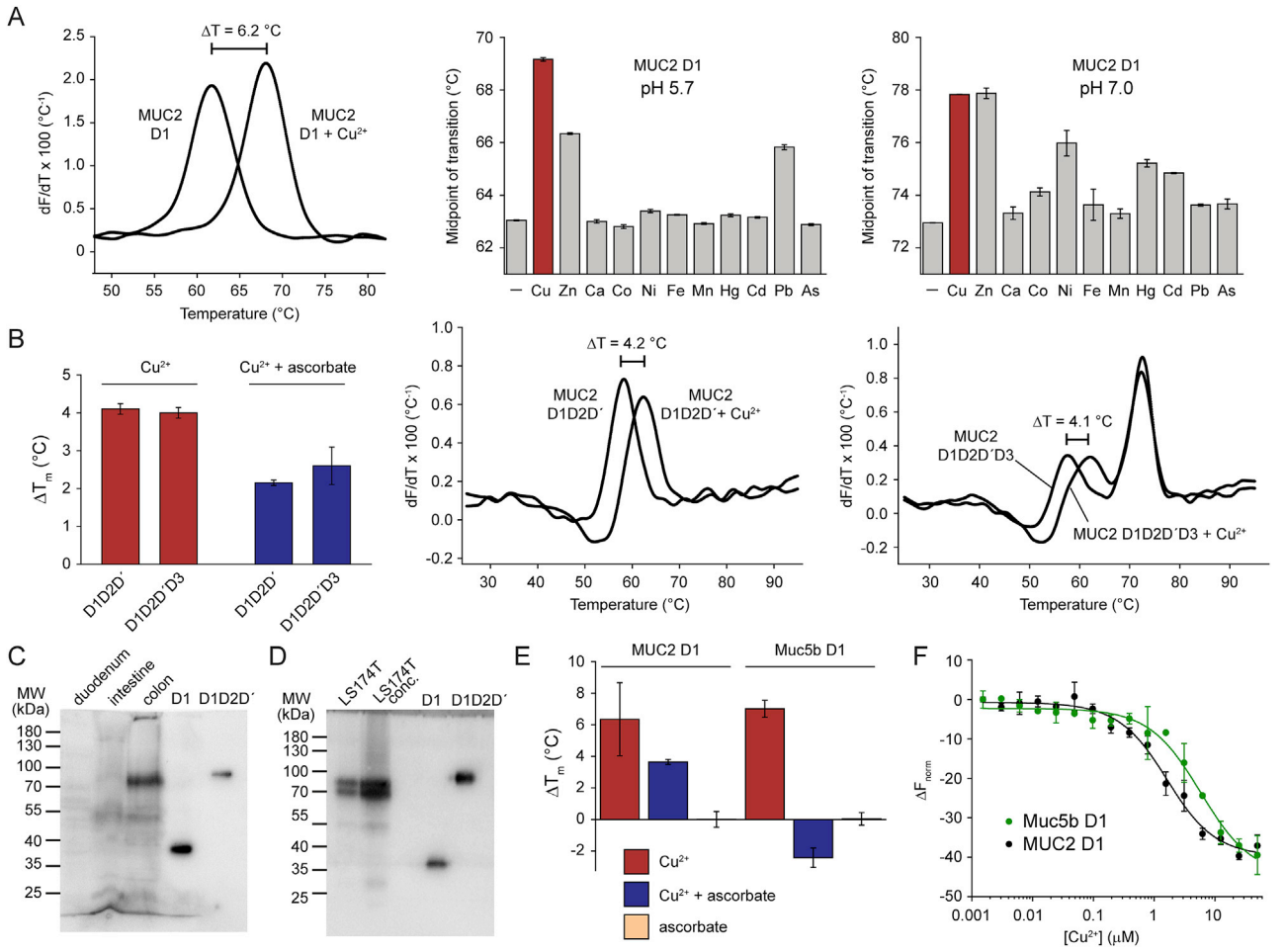

Figure S4. Cu^{2+} binds MUC2 D1, longer MUC2 segments, and Muc5b D1, related to Figures 2 and 3

(A) MUC2 D1 at a concentration of 12 μM was subjected to DSF in the presence of 12 μM of metal. The slope of the fluorescence ratio change (dF/dT, in which F refers to the 350/330 nm emission ratio) of one representative measurement is plotted as a function of temperature for the experiment conducted with and without Cu^{2+}. A bar graph shows the midpoints of the thermal denaturation transition for all metals measured. Experiments were conducted in 50 mM MES buffer, pH 5.7, 150 mM NaCl, 0.05% Tween 20 or in 50 mM MOPS buffer, pH 7.0, 100 mM NaCl, 0.05% Tween 20. Metals were supplied as: Cu, copper sulfate; Zn, zinc chloride; Ca, calcium chloride; Co, cobalt chloride; Ni, nickel sulfate; Fe, iron sulfate; Mn, manganese chloride; Hg, mercury chloride; Cd, cadmium acetate, Pb, lead chloride; As, sodium arsenite. Calcium that may have been bound already to the purified protein (Javitt et al., 2020) was not removed prior to the DSF experiment. Data are averages of at least three separate measurements. Errors are SD.

(B) DSF experiments show that copper also stabilizes longer segments of the MUC2 amino-terminal region. Experiments were done at pH 5.7. The spans of the D1D2D′ and D1D2D′D3 segments can be seen in Figure 1A. Bar graphs display the differences between the denaturation temperatures (ΔT_m) with and without Cu^{2+} or Cu^{1+} (produced by supplying Cu^{2+} and ascorbate). The slope of the fluorescence ratio change of one representative measurement each is plotted as a function of temperature for thermal denaturation performed with and without Cu^{2+}. The D1D2D′D3 segment of MUC2 undergoes two distinct thermal transitions measured by DSF; only the transition at the lower temperature is influenced by copper. Protein concentrations were 5 μM. Bar graphs show averages of two separate measurements, and errors are SD.

(C) Urea-extractable material from murine duodenum, small intestine (intestine), and colon were western blotted using an antibody recognizing MUC2 D1. A fragment that migrates similarly to D1D2D′ was detected in the colon. Full-length MUC2 is not visualized in this experiment due to poor extraction from the mucus gel and its large size and cross-linking, which prevent it from entering the gel.

(D) Conditioned medium from LS174T cells was probed by western blot with the MUC2 D1 antibody, revealing fragments with similar migration rates as recombinant D1D2D′. The lane labeled "LS174T conc." is conditioned medium that was concentrated 10-fold prior to loading the same volume on the gel as for the neighboring, unconcentrated lane.

(E) Cu^{2+} increased the midpoint of thermal denaturation of D1 from the respiratory mucin Muc5b (murine ortholog), measured using DSF at pH 5.7. Unlike Cu^{2+}, Cu^{1+}, formed by the addition of Cu^{2+} and ascorbate, did not increase the midpoint of thermal denaturation of D1 from Muc5b. Bar graphs display the differences between the denaturation temperatures (ΔT_m) with and without Cu^{2+} or Cu^{1+} (produced by supplying Cu^{2+} and ascorbate). Data are the averages of four separate measurements, and errors are SD.

(F) MST demonstrated binding of Cu^{2+} to Muc5b D1, present at 0.5 μM. Data are the averages of two measurements. MUC2 D1 data from Figure S1B are shown on the same plot for comparison.

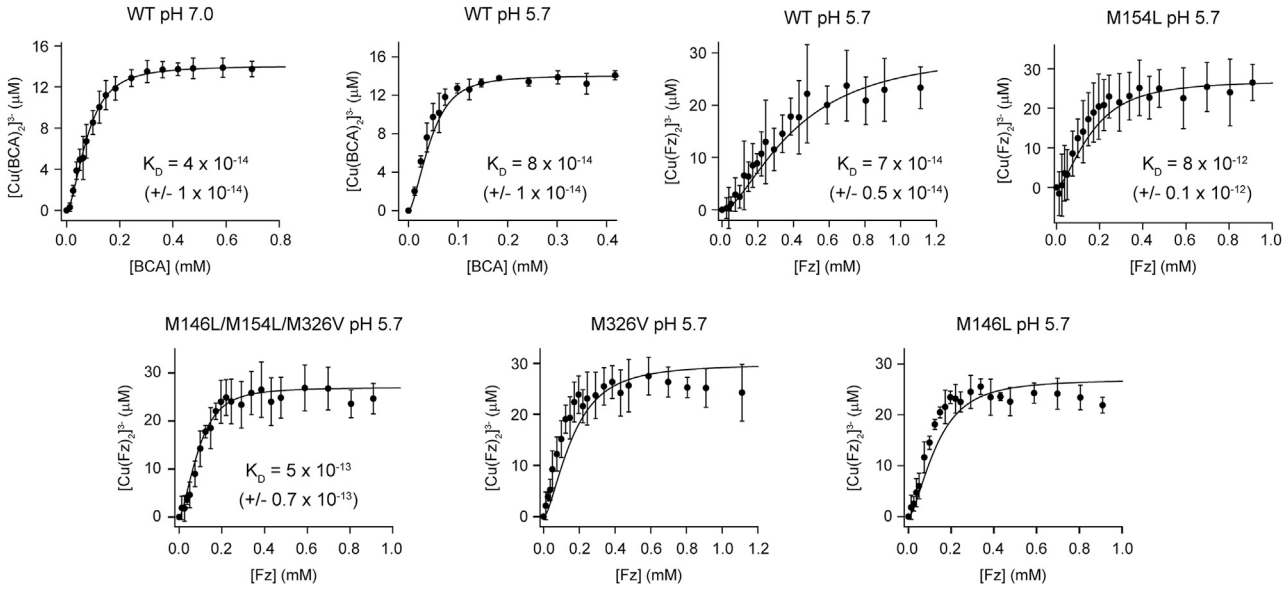

Figure S5. Affinity of MUC2 D1 for Cu^{1+}, related to Figure 3

Competitive binding assays of MUC2 D1 were performed under anaerobic conditions with the colorimetric Cu^{1+} chelators BCA or the weaker binder ferrozine (Fz). Error bars represent SD from the average of triplicate measurements; the lines represent the best fits of Equation 3 in the STAR Methods section to the averaged measurements. Dissociation constants (K_D) shown here were calculated by averaging the values obtained from fits of Equation 3 to the individual titrations. The M146L and M326V mutants did not compete well enough with ferrozine to provide good fits to the data.

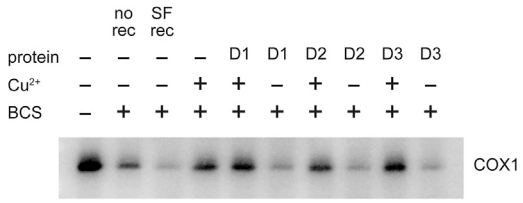

Figure S6. Comparison of COX1 expression after Cu^{2+} addition to copper-starved cells in the presence of MUC2 D1, D2, or D3, related to Figure 5

Caco-2 cells were starved of copper by addition of BCS to the medium where indicated (+) and passaging the cells for 9 days "No rec" indicates the sample that was then harvested with no recovery. To all other samples, serum-free (SF) medium was supplied with the indicated additives, and cells were harvested 3 days later. When present, proteins were at 5 μM and Cu^{2+} was at 1 μM. Cell lysates were subjected to SDS-PAGE and western blotted for COX1. No appreciable differences were seen between addition of copper together with the copper-binding D1 assembly compared to the non-copper-binding assemblies D2 and D3.